Korean J. Chem. Eng., 39(3), 628-637 (2022)
DOI: 10.1007/s11814-021-0910-5

pISSN: 0256-1115
eISSN: 1975-7220

A comprehensive study on the applicability of tea leaves and rice straw as novel sorbents for iron and manganese removal from running water in a fixed-bed column

Allahyar Daghbandan†, Behrooz Abbasi Souraki, and Mohammad Akbari Zadeh

Department of Chemical Engineering, Faculty of Engineering, University of Guilan, Rasht, Iran
(*Received 11 May 2021 • Revised 22 June 2021 • Accepted 20 July 2021*)

Abstract−Iron and manganese, among the most abundant elements on earth, enter bodies of water in the solution form through acid rain. High content of these metals causes sediment, turbidity, taste, and color in the water, thus leading to adverse effects on human health and quality of treated water. In this study, tea leaves and rice straw were used to remove iron and manganese from running water in a fixed-bed column. The effects of the flow rate, sorbent doses, pH, temperature, and the initial concentration of iron and manganese ions were studied. The breakthrough curve and mathematical models, including neural network, genetic algorithm, Thomas and Adams-Bohart models, were drawn upon to evaluate the results. According to the results, the best adsorbent performance was obtained at Initial concentration: 5 mg/l, flow rate: 10 ml/min, pH: 7.9, Adsorbent dosage: 0.1 mg, Retention Time: 20-150 min and Temperature: 30 °C. The percentage of the removed adsorption was 87.7 and 81.3 for rice straw and tea leaves for iron removal and 83.1 and 72.1% for manganese, respectively. The adsorption capacity of rice straw is greater than that of tea leaves, and rice straw absorbs more iron ions than manganese.

Keywords: Iron, Manganese, Tea Leaves, Rice Straw, Fixed Bed Column, Artificial Intelligence

INTRODUCTION

Humans are continuously exposed to iron and manganese through food, air, and water [1]. Iron and manganese are found to be among the most abundant elements in soil and in the earth's crust [2]. These elements may enter water in their soluble form through acid rain. Excessive amounts of these elements create sediment, turbidity, taste, and color in the water [3]. Due to undesirable effects of these ions on the quality of water, scientific methods are required to remove them [4,5]. The permissible level of Mn is 0.5 mg/L and drinking water standards set the maximum allowable amount of iron at 0.3 mg/L, as higher levels are undesirable for industrial and domestic use [6]. Due to the importance of Mn and Fe ions in environmental and health issues, their removal from drinking water by surface adsorption by a low-cost adsorbent is discussed [3]. One of these methods emphasizes the absorption of heavy metals from water through contact with different plant parts, such as stems, leaves, roots, flowers, skin, and fruits [7]. Natural or modified biomaterials, by-products, or waste from industrial and agricultural operations are among the most important sources of low cost adsorbent [7,8]. One of the most famous of these plants is tea, where the elements are stored in elderly leaves [9-11]. Rice is also a tolerant plant in acidic soils [12-14]. Therefore, a new, inexpensive and cost-effective method is needed to remove metal ions from running water [15]. Among the methods available for the removal of metallic elements, the adsorption process is preferred because it is economical, flexible, high efficient and reproducible [15]. Most studies so far performed in this regard utilize batch processes [16,17]. The removal of methylene blue from water by tea waste active with H_3PO_4 (H-AC), KOH (K-AC) and $ZnCl_2$ (Z-AC) agents has been studied by Toli et al. EDX, FT-IR, FESEM, XRD and TGA analyses were performed on the adsorbents and the results showed that the adsorption capacity of H-AC adsorbent to remove methylene blue is higher than the others [18]. Hameed and El-Khaiary used rice straw char to remove malachite green, and the results showed that rice straw char is suitable for removing dye from aqueous solutions [19]. However, for elimination of metal ions from water sources by adsorbents, the batch process has been used more commonly than the continuous process. In the fixed-bed method, the adsorbent is always in the vicinity of the fresh solution. Nassar et al. studied the adsorption of iron and manganese on palm fruit bunch and maize bob in a fixed-bed column [1]. Patel conducted a comprehensive study on the continuous fixed bed adsorption process. In this study, which was conducted in 2019, he examined more than 100 titles of articles [15]. The use of tea waste to remove Cu and Pb from wastewater was investigated by Emersing et al. The experiments were performed in a fixed bed column and the effect of adsorbent dose, initial concentration, pH, particle size and Breakthrough curves was investigated. The results showed that tea waste is effective in removing Cu and Pb ions from wastewater [20]. More recently, many studies have been performed on biosorption [13,17,21]. For instance, breakthrough curves have been applied to analyze a fixed-bed column, indicating a significant effect on the column's performance [21-23]. Various mathematical models, including Thomas, Adams-Bohart, and Yoon-Nelson, have been developed for a fixed-bed process [1,4,21,24]. The efficiency of various biosorbents has been studied by many researchers [3,20,21]. In this study, given the wide areas of tea and rice cultivation in Gilan Prov-

†To whom correspondence should be addressed.
E-mail: daghbandan@guilan.ac.ir

ince in the north of Iran, and the inevitable production of waste, the use of tea leaves and rice straw as raw materials for the production of adsorbents is suggested. Then, the impacts of initial concentration, flow rate [23], contact time, adsorbent dosage, temperature, and pH [20] on the removal of iron and manganese [1,5,25] were studied. The designed pilot can control the temperature and flow rate to perform the absorption process in a continuous fixed-bed method. The process temperature in the absorption source and column was controlled through a thermostat and a heat source. A coded flow meter was used in the Arduino software environment to control the flow rate. The effect of pH changes was also investigated. For the analysis of the breakthrough curves, Thomas [21] and Adams-Bohart [24] models were used. Moreover, the group method of data handling (GMDH) [26] was applied to estimate the output concentration of the metal ions. To compare the predicted and experimental data, three parameters, i.e., the coefficient of determination (R^2), the mean squared error (MSE), and the root-mean-square error (RMSE), were calculated. A wide range of optimization methods available in the literature, such as evolutionary algorithms including the genetic algorithm (GA) [27], were used for the optimization of the parameters influencing the output concentration using input-output datasets [28].

MATERIALS AND METHODS

1. Preparation of Adsorbent

Tea leaves (TL) and rice straw (RS) were used as biosorbent. Samples were collected from tea plants and rice paddies in the north of Iran. At first, samples were washed with running water and then boiled several times until colorless. Afterwards, adsorbents were oven-dried for 24 hour at 70 °C, then ground and sieved for preparation of the required sample size. The fraction between 0.5 and 0.6 mm was chosen for all experiments. The dried powder was stored in sealed polythene bags in desiccators before use [19,20].

2. Preparation of Metal Solutions

For preparation of synthetic water solutions, analytical grades of Iron (III) chloride (with a chemical formula $FeCl_3 \cdot 6H_2O$) and manganese (II) chloride (with a chemical formula $MnCl_2 \cdot 4H_2O$) were dissolved in deionized water to obtain stock solutions (1,000 mg/L). The solution was diluted so as to obtain the specific concentration of Fe and Mn ions [2].

3. Characterization of Adsorbents

For determination of the samples' bioactive components, gas chromatography-mass spectrometry was used (GC-MS (GC7890-MS5975, Agilent, USA)). Analysis of GC-MS was conducted on a GC-MS, including an AOC-20i auto-sampler. Also, a chromatograph was interfaced with a mass spectrometer. To obtain the specific surface area and pore volume, Brunauer-Emmett-Teller (BET) analyzer (BELSORP MINI II, Japan) was applied. To measure distribution of pore size, Barrett-Joyner-Halenda method (BJH) was used. For examination of the surface morphology of the samples, a scanning electron microscope was used (SEM (HITACHI S-3500N, Japan)). The elemental chemical compositions were determined by energy dispersion spectroscopy (EDS) with an EDAX spectrometer. The spectra of adsorbents were recorded by Fourier transform infrared spectroscopy (FT-IR (JASCO, FT-IR-4700 type A)).

4. Main Setup

Fixed-bed adsorption was studied to evaluate the column performance of Fe and Mn removal. Experiments were performed in a vertical down flow column that was fitted with different adsorbents (i.e., TL and RS) for other specified parameters, including flow rate, dosage of adsorbent, pH, temperature, and the initial ion concentration. A feed water reservoir (20-lit capacity) was considered with a heat source inside, whose temperature was controlled by a thermo regulator. Moreover, the inlet stream was placed over the reservoir, and the feed flow was pumped by a variable flow pump (WS123). For the next step, the stream was conducted by a three-way pipe. One stream returned to the feed water reservoir,

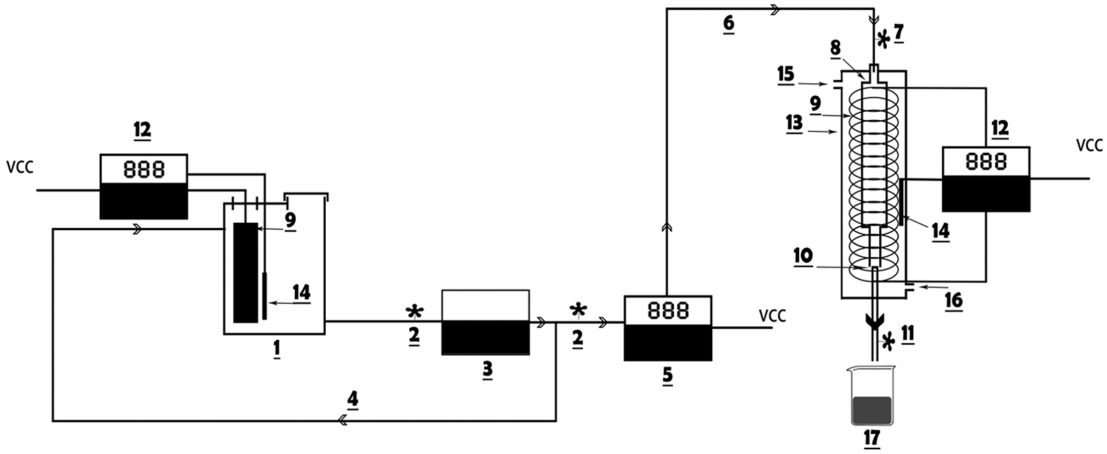

Fig. 1. Schematic diagram of the lab-scale column.

1. Feed storage
2. Control value
3. Water circulation pump (WS123)
4. Back flow
5. flow meter
6. Delivery pipe
7. Inlet value
8. Absorption column (made of Pyrex)
9. Heat source
10. Absorbent holder base
11. Outlet value
12. Thermo regulator
13. Outer shell
14. Temperature sensor
15. Inlet water stream
16. Outlet water stream
17. Sample collector

and the other entered the flow meter. Subsequently, the stream entered the top of the column. The absorption column had an outer protective body that was covered by a heating element. The region between the shell and the tube was filled with water, where a thermo regulator was used for controlling the temperature as well. At the column outlet, the samples were collected at different times for each test. The flow was stopped once the column was fully marked by C_t=C_0. Before beginning the next test, distilled water was used for washing the column. Fig. 1. displays the schematic diagram of the lab-scale column, observed in earlier studies as well [21,29-31].

5. Experimental Study of the Fixed Bed

To evaluate the column performance for Fe and Mn removal, fixed-bed adsorption was studied. The column was also studied to understand the effects of initial concentration, flow rate, adsorbent dose, temperature, and pH. Moreover, experiments on the continuous-flow adsorption were carried out in a glass column (with an internal diameter of 1 cm and a length of 50 cm). The influent concentration of Fe and Mn (C_0) was 2, 5, and 10 mg/l, respectively. The mass of the tea leaves and the rice straw in the column was 0.05, 0.1, and 0.2 g at depths of 3, 5, and 10 cm, respectively. The flow rate varied from 5 to 10 and to 20 ml/min. Temperature was maintained at 15, 30, and 45 °C, while the pH value was kept at 7.9, 3.14, and 12.34, respectively. In all of the experiments, pH value of the solution was adjusted by addition of 0.1 mol/l of HCL or NaOH. The processes were oscillated from 2, 5, 10, 20 … to 720 min, respectively. Once the column was fully marked by C_t=C_0, the flow stopped. For each test, samples were collected at a volume of 15 ml for analysis using atomic adsorption (Agilent 240-280 Series AA) as effluent Fe and Mn ion concentration (C_t).

The breakthrough curve is usually described as the ratio of the ion concentration at the outlet to the column inlet ratio (C/C_i) in the function of time for the fixed-bed column. The amount of adsorbed Fe and Mn was calculated by Eq. (1):

$$q_{total}=\frac{Q*A}{1{,}000}=\frac{Q}{1{,}000}\int_0^{t_{total}} C_{ad}dt=\frac{Q}{1{,}000}\int_0^{t_{total}}(C_0-C)dt \quad (1)$$

where q_{total} indicates the maximum absorbed mass from the column in mg/g, Q is the flow rate circulating through the column in ml/min, A is the area under the breakthrough curve in m^2, t_{total} is the total time in min, C_{ad} is the absorbed removal concentration in mg/L, and C_0 is the Fe and Mn ions initial concentration in mg/L. The area under the breakthrough curve indicates the absorbed metals total mass: q_{total}. The column equilibrium capacity was obtained by Eq. (2):

$$q_{eq}=\frac{q_{total}}{m} \quad (2)$$

where m is the dry adsorbent mass, and m_{total} is the total mass absorbed into the column, which is obtained using Eq. (3):

$$m_{total}=\frac{C_0 Q t_{total}}{1{,}000} \quad (3)$$

The percentage of the removed adsorption (%R) was calculated from Eq. (4):

$$\%R=\frac{q_{total}}{m_{total}}*100 \quad (4)$$

6. Mathematical Description

Usually, a mass transfer-based mathematical model is used to describe adsorption [32,33]. For this purpose, various models have been presented in the references [22]. The output concentration for Fe and Mn ions in running water was used as the desired output of the mathematical model. The most famous and widely applied models used in column performance theory [22] are Thomas [21] and Adams-Bohart [33]. For construction of the feed-forward GMDH-type neural network, experimental data were used. Prediction and training errors were calculated by multi-objective optimization [26,28]. Among various optimization methods inspired by nature, the genetic algorithm is one of the most evolved. The most important parameters in the GA are as follows: initial population size, generation, cross-breeding probability, mutation probability, and selection method [27,34,35].

RESULT AND DISCUSSION

1. Characterization of the Biosorbent

1-1. Determination of Bioactive Compounds by GC-MS

The GC-MS analysis for a methanolic extract of the samples showed compounds that mainly comprise hydrocarbons, fatty acids, esters, steroids, phenols, and nitrogen. Twelve and fifteen chemical constituents were identified in the TL and RS methanolic extract, respectively. The chemical information, such as chemical name, molecular weight, and structure, of the important components of TL and RS is shown in Table S1 (Supplementary Information).

TL major compound was caffeine (88.34%), belonging to nitrogen compounds class. Also, phthalate (23.80%) is a major chemical constituent of RS.

1-2. Surface Area and Pore Diameter (BET and BJH Analysis)

N_2-based adsorptive characterization is one of the most widely used techniques. Table 1 shows the surface area, volume and pore size of TL and RS and their adsorption/desorption isotherms are also shown in Fig. S1.

As classified by IUPAC, nitrogen adsorption isotherms of TL and RS are type III in addition to an H3 type hysteresis loop, which indicates the presence of mesoporous texture. Accordingly, type H3 hysteresis usually exists on solids with a very wide pore size

Table 1. Surface area, volume and pore size of TL and RS

Sample	Surface area				Total pore volume (m^3/g)	Pore size (nm)
	BET (m^2/g)	Langmuir (m^2/g)	t-Plot (m^2/g)	BJH plot (m^2/g)		
TL	0.28866	0.3964	0.237	1.5176	0.0037707	52.25
RS	3.7052	3.0634	1.3938	6.3386	0.01735	18.731

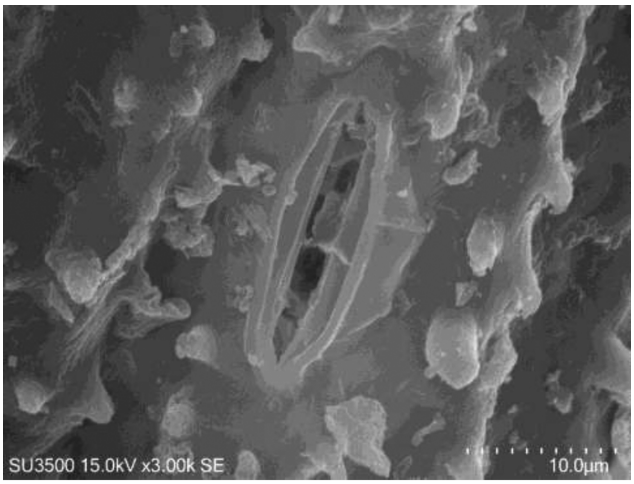

(a) Original RS

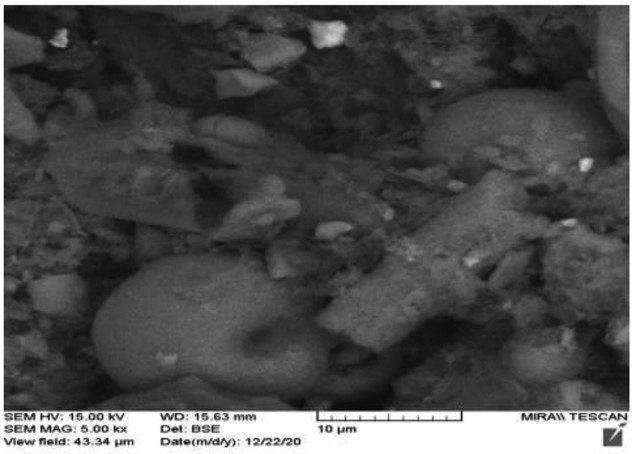

(b) Fe and Mn loaded RS

Fig. 2. Scanning of electron microscope (SEM) images of RS samples.

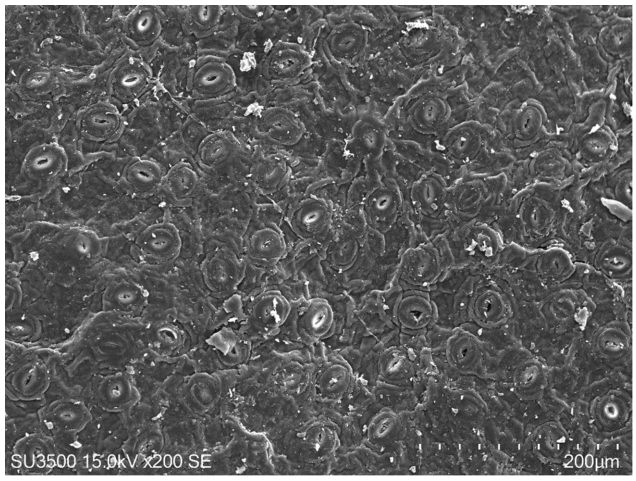

(a) Original TL

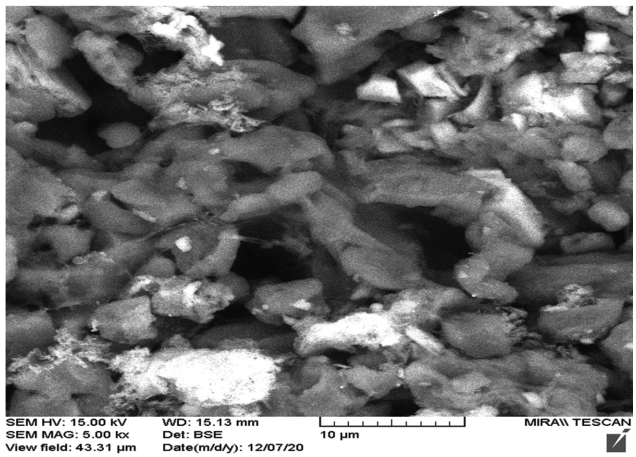

(b) Fe and Mn loaded TL

Fig. 3. Scanning of electron microscope (SEM) images of TL samples.

distribution, not signifying any limiting adsorption at high P/P_0 [13,36,37].

1-3. Scanning Electron Microscopy (SEM) Combined with X-ray Energy Dispersive Spectrometer (EDX)

The surface morphology of original and metal loaded RS and TL samples is shown in Figs. 2 and 3, respectively. The EDS spectra were executed to prove the effective loading of Fe and Mn onto biosorbents as shown in Fig. S2 and S3.

Original RS and TL retained a smooth surface as shown in Fig. 2(a) and 3(a). Meanwhile, the samples treated with Fe and Mn, shown in Fig. 2(b) and 3(b), had a rougher surface and were covered with small flocculent material which resembled fibers. This phenomenon is likely due to an inorganic layer formed on the surface of adsorbents by Mn and Fe ions. As shown in Fig. S2(a) and S3(a), the main elements existing in the primary RS and TL were carbon and oxygen elements, originating from the lignocellulosic nature of biosorbents. Moreover, a new peak of Fe and Mn in TL-Fe|Mn, and RS-Fe|Mn was found that indicated Fe with 0.5592 and 0.5679 wt%, respectively (Fig. S2(b) and S3(b)). Such findings suggest that TL and RS could adsorb Fe and Mn ions from the solution. This also assumes that the adsorption process of Fe and Mn ions onto biosorbents may be physical [5,10,16,37,38]. Generally, rough surfaces and extensively distributed pores can suggest a larger surface area and more attached metal sites.

1-4. Fourier Transform Infrared Spectra (FT-IR)

Fig. 4 shows the FT-IR spectra of RS and TL before and after metal sorption. Detailed band variation data of different sorption RS and TL peaks are presented in Table S2. The FTIR spectrum of the TL and RS has an absorption band at the 4,000-2,500 cm^{-1} wave number, which is a vibration of C-H and O-H, and 2,500-1,500 cm^{-1}, The wave number indicates the presence of C=O vibration and 1,500-650 cm^{-1}, which is C-O, C-C and C-N. RS also has a variety of carbonaceous compounds [39,40].

As observed in the analysis of rice straw and tea leaves, these sorbents have a variety of carbonaceous compounds [41,42]. The strong peaks at 3,433 cm^{-1} are indicators of the presence of O-H stretching vibration of aliphatic compounds in the RS and TL lignin structure [43]. Briefly, compared to the original TL and RS, the band frequency after metal sorption indicated variation at some sorption bands, which suggests that those functional groups are

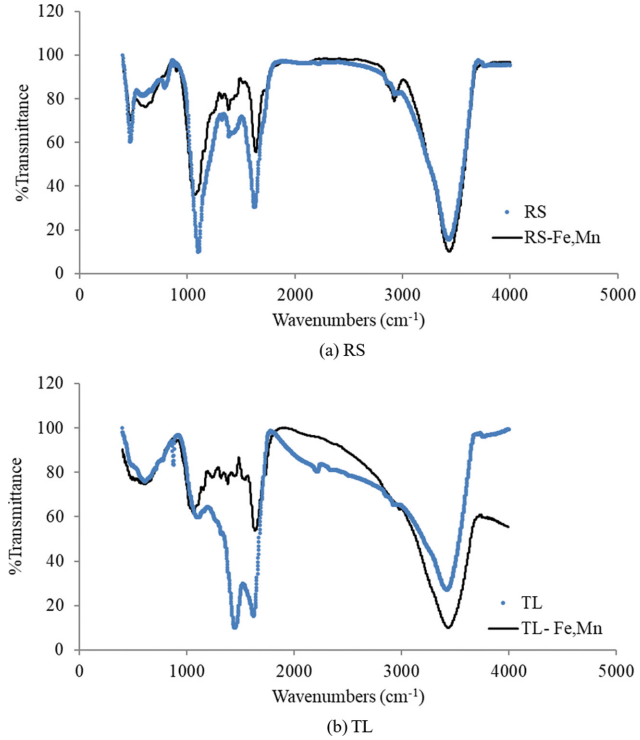

Fig. 4. FT-IR spectral characteristics of (a) RS and (b) TL before and after Fe and Mn ions sorption.

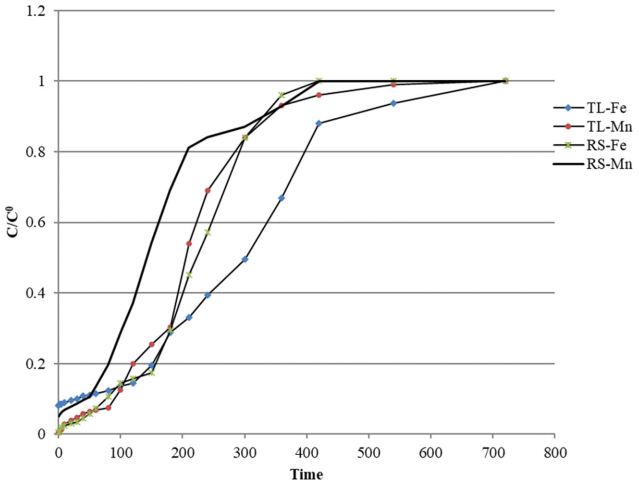

Fig. 5. Breakthrough curves: effect of time on Fe and Mn adsorption with TL and RS (C_0=5 mg/L, m=0.2 g).

possibly involved in the adsorption process. The existence of O-H and C-O bonds signifies that the activated carbon produced is prone to more polarization. Thus the derived TL and RS can be selected as an adsorbent [5,17,37].

2. Effect of Retention Time

To evaluate the column performance for Fe and Mn removal, fixed-bed adsorption was studied. The column was also studied to understand the effects of initial concentration, flow rate, adsorbent dose, temperature, and pH. The Fe and Mn ion removal percentages at various oscillation retention times with RS and TL are presented in Table 2 and Fig. 5. The influent concentration of Fe and Mn (C_0) was 5 mg/l, the mass of the TL and the RS in the column was 0.1 g, and the flow rate was 10 ml/min. The temperature was maintained at 30 °C and the pH value was kept at 7.9. The processes shifted from 2, 5, 10, 20 … to 720 min, respectively.

Regarding the sorbents, metal decreased sharply for the first 60 min of contact time. With a further passage of time, a progressive decrease occurred in the sorption kinetics. The achievement for metal removal was gained at 720 min for TL-Fe/Mn and RS-Fe/Mn. Initially, adsorption occurred rapidly because adsorptive sites

Table 2. Effect of time on Fe and Mn ions adsorption in the fixed-bed column

Adsorbent	Absorbed	Z (cm)	t_1 (min)	t_2 (min)	q_{eq} (mg/g)	%R
TL	Fe	10	40	360	67.29	74.09
	Mn	10	10	300	58.87	70.72
RS	Fe	10	5	240	72.17	90.31
	Mn	10	40	180	62.38	78.05

Table 3. The Thomas and Adams-Bohart models parameters for Fe and Mn adsorption by TL and RS

Model	Adsorbent	Absorbed	Z (cm)	t_1 (min)	t_2 (min)	K_{Th} (ml/mg.min)	q_0 (mg/g)	R^2
Thomas	TL	Fe	10	40	360	0.0027	48,793.75	0.98
		Mn	10	10	300	0.0054	33,834.65	0.99
	RS	Fe	10	5	240	0.0051	73,794.76	0.98
		Mn	10	40	180	0.0067	47,654.84	0.99
Model	Adsorbent	Absorbed	Z (cm)	t_1	t_2	K_{BA} (L/mg min)	N_0 (mg/L)	R^2
Adams-Bohart	TL	Fe	10	40	360	0.0019	1,498.14	0.98
		Mn	10	10	300	0.0037	1,039.95	0.97
	RS	Fe	10	5	240	0.0042	2,036.89	0.96
		Mn	10	40	180	0.0045	1,340.85	0.98

Table 4. Effect of initial concentration on Fe and Mn ion adsorption in the fixed bed column (flow rate: 10 ml/min, sorbent dose: 0.1 g, pH: 7.9, and temperature: 30 °C)

Adsorbent	Absorbed	C (mg/L)	q_{eq}	%R
TL	Fe	10	261.2	62.2
	Fe	5	130.2	62
	Fe	2	50.6	70.3
	Mn	10	116.7	48.6
	Mn	5	115.3	54.9
	Mn	2	50.6	60.2
RS	Fe	10	155.4	51.8
	Fe	5	220.7	73.6
	Fe	2	31.2	77.9
	Mn	10	154.2	51.4
	Mn	5	139.6	66.6
	Mn	2	31	77.7

were available in high numbers.

3. Mathematical Description

The column performance theory made use of the Thomas and Adams-Bohart mathematical models [22]. The fixed bed process was done for TL-Fe|Mn and RS-Fe|Mn binary systems. The parameters calculated and presented in Table 3 are as follows: Thomas speed constant (K_{Th}) maximum absorption capacity (q_0) parameters in Thomas model and kinetic coefficient (K_{BA}) as well as volumetric absorption capacity (N_0) parameters in Adams-Bohart model, and coefficient of determination (R^2).

Overall, breakthrough curves and Thomas and Adams-Bohart models results showed that the adsorption capacity of rice straw is greater than that of tea leaves, and rice straw absorbs more iron ions than manganese.

4. Effect of Initial Concentration

The influent concentration of Fe and Mn (C_0) was 2, 5, and 10 mg/l. The adsorption percentage of the metals decreased as the initial concentration of ion in the aqueous solution increased (Table 4), suggesting that when ion concentration is low, the ratio of the surface active sites to the total metal ions in the solution is high. Therefore, all ions can interact with RS and TL; this causes their removal from the solution. At 2 mg/L initial concentration, the residual concentration decreased significantly (i.e., to 0), which is lower than the levels of Fe and Mn permitted by WHO for drinking water [6].

5. Effect of the Flow Rate

The column was run with flow rates of 5, 10, and 20 ml/min. As shown in Table 5, the metals adsorption percentage decreased whenever the flow rate increased, owing to decline in contact time that itself limits the contact between the metal ions and the adsorbent. The same results were obtained for of Fe and Mn adsorption in the fixed-bed system when RS and TL were used as adsorbing media in the column [1,37,38].

6. Effect of Adsorbent Dosage

For final designing of optimum treatment systems, several experiments were performed with adsorbent dosages of 0.05, 0.1, and 0.2 g. The metal adsorption percentage decreased when the adsorbent dosage decreased (Table 6). With further rise in sorbent doses, metal removal from the solution would not be significantly affected [5].

Table 5. Impact of flow rate on Fe and Mn ion adsorption in the fixed bed column (Initial concentration: 5 mg/l, Sorbent dose: 0.1 g, pH: 7.9, and temperature: 30 °C)

Adsorbent	Absorbed	Flow rate (ml/min)	q_{eq}	%R
TL	Fe	5	195	81.3
	Fe	10	130.2	62
	Fe	20	28.4	31.6
	Mn	5	173.1	72.1
	Mn	10	115.3	54.9
	Mn	20	69.9	33.3
RS	Fe	5	157.9	87.7
	Fe	10	220.7	73.6
	Fe	20	91.7	30.5
	Mn	5	274.3	83.1
	Mn	10	139.6	66.6
	Mn	20	101.7	48.4

Table 6. Effect of adsorbent dosage on Fe and Mn ion adsorption in the fixed bed column (Initial concentration: 5 mg/l, flow rate: 10 ml/min, pH: 7.9, and temperature: 30 °C)

Adsorbent	Absorbed	Adsorbent dose(mg)	q_{eq}	%R
TL	Fe	0.05	130.6	31.1
	Fe	0.1	130.2	62
	Fe	0.2	50.5	72.2
	Mn	0.05	134.8	32.1
	Mn	0.1	115.3	54.9
	Mn	0.2	63.2	60.2
RS	Fe	0.05	330.6	55.1
	Fe	0.1	220.7	73.6
	Fe	0.2	102.9	82.3
	Mn	0.05	160.4	38.2
	Mn	0.1	139.6	66.6
	Mn	0.2	67.6	75.1

7. Effect of Temperature

As shown in Table 7, the adsorption capacity increased slightly with increase in the temperature from 15 to 30 °C, indicating the endothermicity of the adsorption process. The increased sorption may have occurred due to various factors, including a decrease in the thickness of boundary layer, which caused a decline of mass transfer resistance. The development of a swelling effect on the internal structure of the sorbent gave rise to a further penetration of metal cations [47]. An increase in inactive sites occurred due to bond rapture [48]. However, a further rise in temperature to 45 °C caused a decline in the metal adsorption percentage.

8. Effect of pH

The impact of pH variation on metal ion absorption with RS and TL is presented in Table 8. The effect was tested at pH values

Table 7. Effect of temperature on Fe and Mn ion adsorption in the fixed-bed column (Initial concentration: 5 mg/l, sorbent dose: 0.1 g, pH: 7.9, and flow rate: 10 ml/min)

Adsorbent	Absorbed	T (°C)	q_{eq}	%R
TL	Fe	15	65.5	31.2
	Fe	30	130.2	62
	Fe	45	90.3	43
	Mn	15	62	29.5
	Mn	30	115.3	54.9
	Mn	45	86	41
RS	Fe	15	127.2	42.4
	Fe	30	220.7	73.6
	Fe	45	179.1	59.7
	Mn	15	75.8	36
	Mn	30	139.6	66.5
	Mn	45	112.9	53.8

Table 8. Effect of pH on Fe and Mn ion adsorption in the fixed-bed column (Initial concentration: 5 mg/l, sorbent dose: 0.1 g, temperature: 30 °C, and flow rate: 10 ml/min)

Adsorbent	Absorbed	pH (-)	q_{eq}	%R
TL	Fe	3.14	65.7	27.4
	Fe	7.9	130.2	62
	Fe	12.13	103.97	43.3
	Mn	3.14	72.7	30.3
	Mn	7.9	115.3	54.9
	Mn	12.13	57.3	31.8
RS	Fe	3.14	173.9	48.3
	Fe	7.9	220.7	73.6
	Fe	12.13	181.6	50.4
	Mn	3.14	75.8	36
	Mn	7.9	139.6	66.6
	Mn	12.13	112.9	53.8

of 3.14, 7.9, and 12.13. It is known that pH plays a very significant role in metal ions adsorption and in the solubility of metals [49]. With a rise in pH values from 3.14 to 7.9, a rise occurred in the removal percentage of metal ions as well. At acidic pH, the removal efficiency was low, likely due to the competition between H^+ and metal ions [50]. It is notable that the adsorption percentage of metals falls at higher pH values (pH=12.13). This is because the precipitation of a metal, such as Fe $(OH)_3$, occurs owing to the presence of OH^- ions in the adsorption medium [51]. These findings are in accordance with those acquired for other biomass materials, i.e., rice husk char [5,37,49].

9. Modeling of Output Concentration Using GMDH-type Neural Network

The feed-forward GMDH-type neural network for the outlet concentration of Fe and Mn ions in running water was constructed using experimental data. Also, the prediction error and training error was calculated using multi-objective optimization. The structural parameters of GMDH-type neural network are summarized in Table S3. The GMDH values of TE and PE of deterministic optimal design points A, B, and C are presented in Table S4. A and B

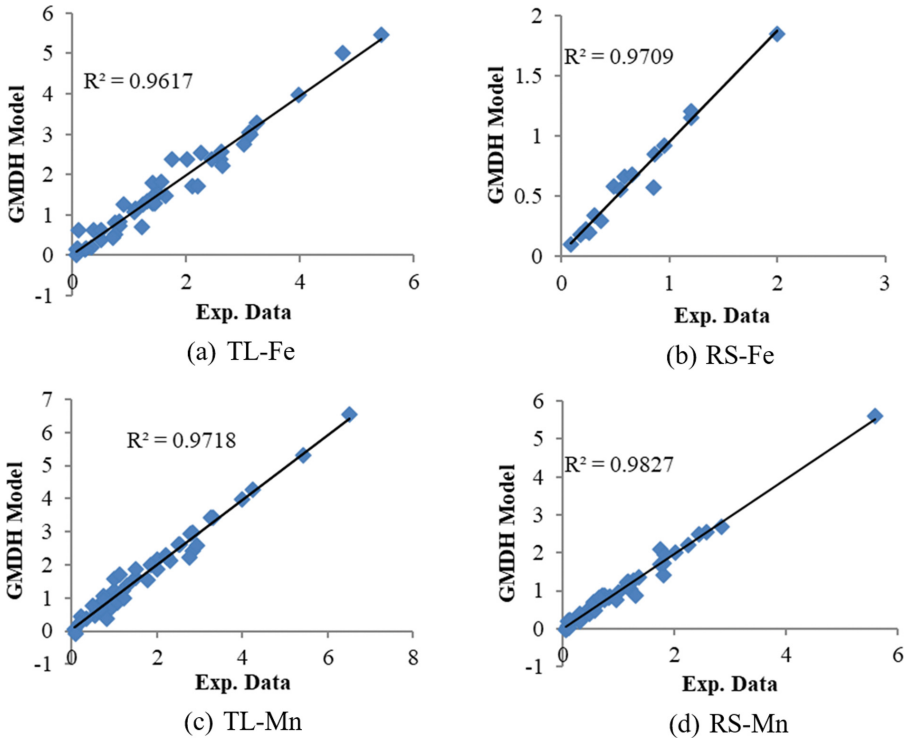

Fig. 6. Comparison between actual output and GMDH output of design point C of processes ((a) TL-Fe; (b) RS-Fe; (c) TL-Mn and (d) RS-Mn).

Table 9. Optimum values of effective parameters on output concentration of samples

Input						Output
Temperature (°C)	pH —	Concentration (mg/l)	Adsorbent dosage (mg)	Time (min)	Mass flow (ml/min)	Final concentration of samples (ppm)
24-37	5.6-9	0-6.7	0.08-0.1	20-150	6.5-12	0

Points represent the GMDH model with minimum prediction and training errors, respectively. However, the design point C depicts tradeoff in such models; it can be selected as the best optimal model.

Regarding this approach, training (TE) and prediction (PE) errors were chosen for the bi-objective Pareto optimization approach of the GMDH model, by drawing on the relationships presented in Eqs. (5) and (6), respectively.

$$TE=\sum_{i=1}^{n}(Y_{i,\,exp}-Y_{i,\,train})^2/\sum_{i=1}^{n}(Y_{i,\,exp})^2 \quad (5)$$

$$PE=\sum_{i=1}^{n}(Y_{j,\,exp}-Y_{j,\,prediction})^2/\sum_{i=1}^{n}(Y_{j,\,exp})^2 \quad (6)$$

The optimal structures for the developed GMDH Type-Neural Network with 4 and 5-hidden layers are shown in Table S5, where a, b, c, d, e, f, and g stand for parameters affecting the output concentration.

The experimental and predicted data were now compared through GMDH model output. The model accepted all input variables. The outputs generated by the GMDH model with experimental data are presented in Fig. 6. The experimental and predicted values of the adsorption process were in close agreement, as shown in Fig. 6.

The obtained model is simply applicable to the adsorption representation process of the metal ions. As a consequence, the proposed GMDH model can be adequately used for prediction of the experimental data.

10. Optimization of Influential Parameters on Final Concentration by Genetic Algorithm

The genetic algorithm is used for optimization of the influence parameters on output concentration. The values of the optimized parameters influencing the output concentration are given in Table 9.

The effect of each parameter on output concentration in optimum condition is presented in Fig. 7. In these diagrams, other parameters are considered in optimum values.

The curve for final concentration of samples according to temperature and pH under optimum condition is shown in Fig. 7(a). As displayed, final concentration is minimum when temperature is 35 °C with pH at 8.9. The results of Fig. 7(b) and (c) show that the final concentration of samples had a decline when the initial concentration, time, and flow rate increased; this was while the optimum mass of TL and RS in the column was 0.05-0.1 g [28].

APPLICABILITY OF BIOSORBENT

To find out whether or not the proposed method is applicable to running water, ten control samples (Table 10) were collected

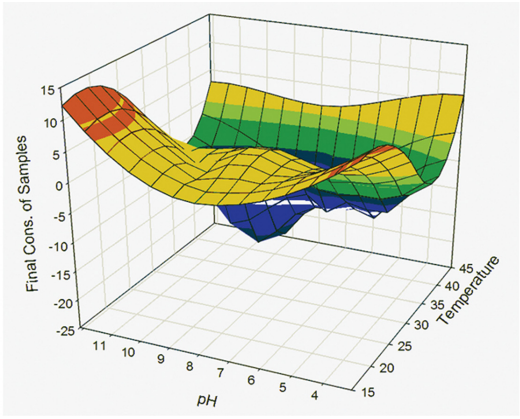

(a) Temperature and Ph

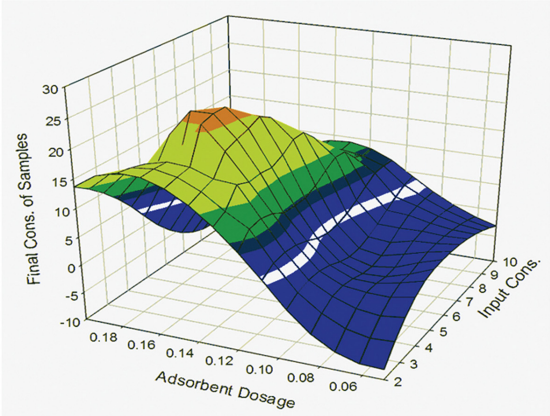

(b) Input concentration and Adsorbent dosage

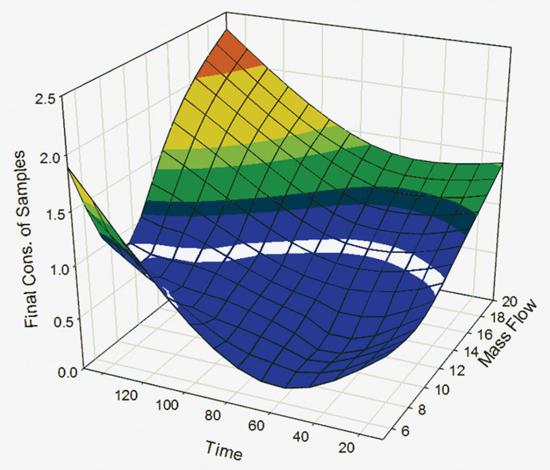

(c) Flow rate and Time

Fig. 7. Effect of each parameter on final concentration of samples in optimum condition.

Table 10. Input-output data sets of running water

Input						Output	
Effective parameters				Initial concentration		Final concentration	
Adsorbent	Temperature (°C)	pH —	Turbidity (NTU)	Color (pt-co)	Fe (ppm)	Mn (ppm)	Fe (ppm)	Mn (ppm)
TL	10.50	8.08	10.90	50	0.05	0.090	0.010	0.030
	11	7.54	0.66	4	0.07	0.040	0.020	0.010
	12.60	8.12	8.30	7	0.03	0.064	0.008	0.009
	14.20	7.39	0.55	3	0.080	0.012	0.020	0.008
	18.20	7.46	0.65	3	0.060	0.013	0.010	0.004
RS	10.50	8.08	10.9	50	0.05	0.090	0.030	0.060
	11	7.54	0.66	4	0.07	0.040	0.040	0.020
	12.60	8.12	8.30	7	0.03	0.064	0.006	0.020
	14.20	7.39	0.55	3	0.080	0.012	0.030	0.004
	18.20	7.46	0.65	3	0.060	0.013	0.015	0.002

from a water treatment plant located in Guilan Province in the north of Iran. Water samples were collected in May 2020. The collected water samples were characterized before treatment. In the treatment procedure, the adsorbent dose was 0.1 g, the maximum contact time was 720 min, and the temperature was 30 °C. Finally, Fe and Mn ion concentrations were measured using an atomic absorption spectrophotometer (Agilent 240_280 Series AA) to determine the adsorption percentage of the metals.

The results of these tests (presented in Table 10) showed that the adsorbents used had acceptable performance under operating conditions.

RESEARCH INNOVATION

The pilot designed to perform the continuous fixed bed absorption process has the capability of controlling the temperature and flow rate. The temperature of the process in the absorption source and column was controlled by a thermostat and a heat source. A flowmeter encoded by Arduino software was used to control the flow rate. The effect of pH changes was also investigated. Modeling and optimization of the process was implemented by artificial intelligence-based methods. The pilot was also tested through real samples taken from Gillan's Water Treatment Plant, North of Iran.

CONCLUSIONS

Based on our experimental results, tea leaves and rice straw are applicable to running water for Fe and Mn ion removal. According to breakthrough curves, rice straw adsorbent can remove 90.31% and 78.05% of iron and manganese ions, respectively. For the latter, 74.09% of iron and 70.72% of manganese removals occurred. The Thomas and Adams-Bohart models sufficiently explained the adsorption of Fe and Mn ions onto TL and RS in column mode. The constants for Thomas and Adams-Bohart mathematical models were calculated: Q_0 for iron and manganese ions removal by TL and RS are 48,793.75, 33,834.65, 73,794.76, 47,654.84, respectively; N_0 is 1,498.14, 1,039.95, 2,036.89 and 1,340.85, in the same order. The results indicate that rice straw is greater than that of tea leaves, and rice straw absorbs more iron ions than manganese. As for the results, the GMDH model is capable of predicting Fe and Mn ion residual concentration in running water with an acceptable accuracy. Under optimum conditions, the concentration of Fe and Mn in running water was minimal. The greatest effect on the concentration of Fe and Mn ions is related to the temperature and the pH of the running water. According to the results, in real systems both TL and RS can efficiently remove Fe and Mn ions within water.

SUPPORTING INFORMATION

Additional information as noted in the text. This information is available via the Internet at http://www.springer.com/chemistry/journal/11814.

REFERENCES

1. M. M. Nassar, K. T. Awida, E. E. Ebrahiem, Y. H. Magdy and M. H. Mehaedi, *Adsorpt. Sci. Technol.*, **21**, 161 (2003).
2. A. bin Jusoh, W. Cheng, W. Low, A. Nora'aini and M. M. M. Noor, *Desalination*, **182**, 347 (2005).
3. S. Maliki, C. Rosnelly, A. Adisalamun, H. Husin and N. Bilqis, Removal of Fe (Ii) in groundwater using rice husk-sourced biosorbent in continuous column adsorption, in Journal Of Physics: Conference Series. IOP Publishing (2019).
4. N. Sylvia, L. Hakim and N. Fardian, Adsorption performance of fixed-bed column for the removal of Fe (II) in groundwater using activated carbon made from palm kernel shells, in Materials Science and Engineering Conference Series (2018).
5. M. E. Goher, A. M. Hassan, I. A. Abdel-Moniem, A. H. Fahmy, M. H. Abdo and S. M. El-sayed, *Egypt. J. Aquat. Res.*, **41**, 155 (2015).
6. O. Akoto and J. Adiyiah, *Int. J. Environ. Sci. Technol.*, **4**, 211 (2007).
7. C. K. Jain, D. S. Malik and A. K. Yadav, *Environ. Processes*, **3**, 495 (2016).
8. S. Hussain, K. Anjali, S. T. Hassan and P. B. Dwivedi, *Appl. Water Sci.*, **8**, 1 (2018).

9. J. Olivier, E. A. Symington, C. Z. Jonker, T. S. Van Eeden and I. T. Rampedi, *S. Afr. J. Sci.*, **108**, 1 (2012).
10. M. Nigam, S. Rajoriya, S. R. Singh and P. Kumar, *J. Environ. Chem. Eng.*, **7**, 103188 (2019).
11. R. Jayabalan, R. V. Malbaša, E. S. Lončar, J. S. Vitas and M. Sathishkumar, *Compr. Rev. Food Sci. Food Saf.*, **13**, 538 (2014).
12. W. Li, J. Du, H. Feng, Q. Wu, G. Xu, S. Shabala and L. Yu, *Planta*, **251**, 1 (2020).
13. F. Xu, T.-T. Zhu, Q.-Q. Rao, S.-W. Shui, W.-W. Li, H.-B. He and R.-S. Yao, *Res. J. Environ. Sci.*, **53**, 132 (2017).
14. S. Jin and H. Chen, *Ind. Crops. Prod.*, **26**, 207 (2007).
15. H. Patel, *Appl. Water Sci.*, **9**, 45 (2019).
16. M. Khobragade and A. Pal, *J. Environ. Chem. Eng.*, **2**, 2295 (2014).
17. S. Ahluwalia and D. Goyal, *Eng. Life Sci.*, **5**, 158 (2005).
18. F. Tuli, A. Hossain, A. F. Kibria, A. Tareq, S. M. Mamun and A. A. Ullah, *Environ. Nanotechnol. Monit. Manag.*, **14**, 100354 (2020).
19. B. Hameed and M. El-Khaiary, *J. Hazard. Mater.*, **153**, 701 (2008).
20. B. Amarasinghe and R. A. Williams, *Chem. Eng. J.*, **132**, 299 (2007).
21. E. Malkoc and Y. Nuhoglu, *J. Hazard. Mater.*, **135**, 328 (2006).
22. M. Khobragade and A. Pal, *Sep. Sci. Technol.*, **51**, 1287 (2016).
23. C. Borba, R. Guirardello, E. Silva, M. Veit and C. Tavares, *Biochem. Eng. J.*, **30**, 184 (2006).
24. A. M. Faizal, S. R. M. Kutty and E. H. Ezechi, *Modelling of Adams-Bohart and Yoon-Nelson on the removal of oil from water using microwave incinerated rice husk ash (MIRHA)*, in Applied Mechanics and Materials. Trans Tech Publ (2014).
25. M. A. Galangashi, S. F. M. Kojidi, A. Pendashteh, B. A. Souraki and A. A. Mirroshandel, *J. Water Process. Eng.*, **39**, 101714 (2021).
26. A. Ivakhnenko and G. Ivakhnenko, *Pattern Recognit. Image Anal.*, **5**, 527 (1995).
27. S. Sivanandam and S. Deepa, *Genetic algorithm optimization problems, in Introduction to genetic algorithms*, Springer, 165-209 (2008).
28. M. Akbarizadeh, A. Daghbandan and M. Yaghoobi, *Int. J. Chemoinform. Chem. Eng.*, **3**, 94 (2013).
29. T. S. Singh and K. Pant, *Sep. Purif. Technol.*, **48**, 288 (2006).
30. Z. Zulfadhly, M. Mashitah and S. Bhatia, *Environ. Pollut.*, **112**, 463 (2001).
31. S. Mohan and G. Sreelakshmi, *J. Hazard. Mater.*, **153**, 75 (2008).
32. H. A. Alalwan, M. N. Abbas, Z. N. Abudi and A. H. Alminshid, *Environ. Technol. Innov.*, **12**, 1 (2018).
33. M. Calero, F. Hernáinz, G. Blázquez, G. Tenorio and M. Martín-Lara, *J. Hazard. Mater.*, **171**, 886 (2009).
34. M. Ilbeigi, M. Ghomeishi and A. Dehghanbanadaki, *Sustain. Cities Soc.*, **61**, 102325 (2020).
35. D. Park, J. Cha, M. Kim and J. S. Go, *Eng. Appl. Comput. Fluid Mech.*, **14**, 180 (2020).
36. K. S. Sing and R. T. Williams, *Adsorpt. Sci. Technol.*, **22**, 773 (2004).
37. Y. Zhang, X. Yue, W. Xu, H. Zhang and F. Li, *J. Hazard. Mater.*, **379**, 120783 (2019).
38. Y. Zhao, M. Huang, W. Wu and W. Jin, *Desalination*, **249**, 1006 (2009).
39. X. Chen, J. Yu, Z. Zhang and C. Lu, *Carbohydr. Polym.*, **85**, 245 (2011).
40. J. S. Cha, J.-C. Choi, J. H. Ko, Y.-K. Park, S. H. Park, K.-E. Jeong, S.-S. Kim and J.-K. Jeon, *Chem. Eng. J.*, **156**, 321 (2010).
41. P. Panneerselvam, N. Morad and K. A. Tan, *J. Hazard. Mater.*, **186**, 160 (2011).
42. M. Ahmaruzzaman and S. L. Gayatri, *J. Chem. Eng. Data*, **55**, 4614 (2010).
43. C. S. Yue, K. H. Chong, C. C. Eng and L. S. Loh, *J. Water Resource Prot.*, **8**, 568 (2016).
44. S. Gueu, B. Yao, K. Adouby and G. Ado, *Int. J. Environ. Sci. Technol.*, **4**, 11 (2007).
45. Y. Li, W. Zhou, B. Hu, M. Min, P. Chen and R. R. Ruan, *Bioresour. Technol.*, **102**, 10861 (2011).
46. E. Erdem, N. Karapinar and R. Donat, *J. Colloid Interface Sci.*, **280**, 309 (2004).
47. S. Mohan and R. Gandhimathi, *J. Hazard. Mater.*, **169**, 351 (2009).
48. K. L. Wasewar, M. Atif, B. Prasad and I. Mishra, *Desalination*, **244**, 66 (2009).
49. H. B. Bradl, *J. Colloid Interface Sci.*, **277**, 1 (2004).
50. T. Altun and E. Pehlivan, *Food Chem.*, **132**, 693 (2012).
51. S.-Y. Lee and H.-J. Choi, *J. Environ. Manage.*, **209**, 382 (2018).

Supporting Information

A comprehensive study on the applicability of tea leaves and rice straw as novel sorbents for iron and manganese removal from running water in a fixed-bed column

Allahyar Daghbandan†, Behrooz Abbasi Souraki, and Mohammad Akbari Zadeh

Department of Chemical Engineering, Faculty of Engineering, University of Guilan, Rasht, Iran
(*Received 11 May 2021 • Revised 22 June 2021 • Accepted 20 July 2021*)

<Research Steps>

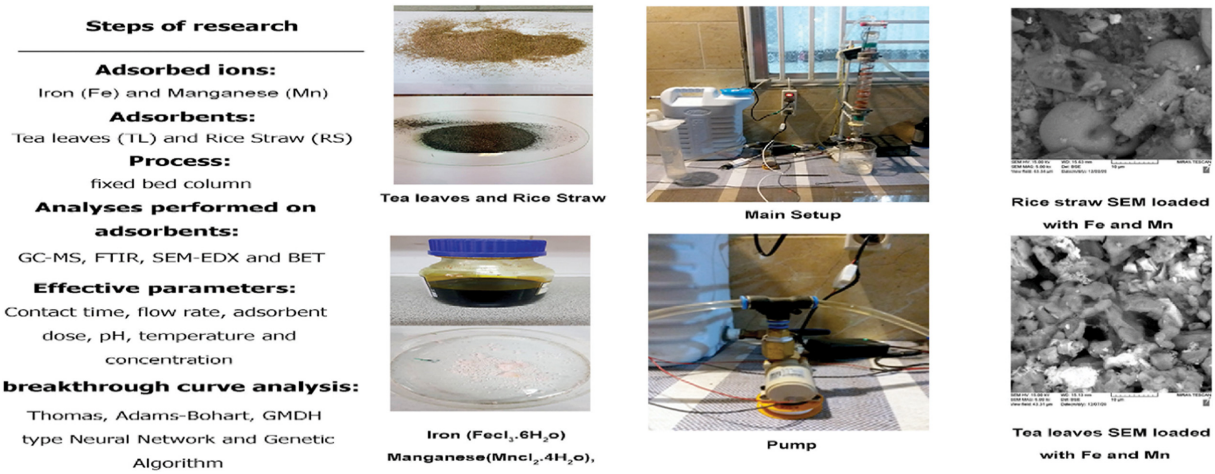

Table S1. Phytocomponents identified in TL and RS by GC-MS

Sample	RT (min)	Area%	Name of compound	Molecular formula	Molecular weight	Class
TL	5.201	0.46	α,β-angelica lactone (2(3H)-Furanone, 5-methyl-)	$C_5H_6O_2$	98.10	Furan
	12.948	3.68	Pyrocatechol, 3-methoxy (1,2-Benzenediol, 3-methoxy-)	$C_7H_8O_3$	140.13	Phenol
	22.614	0.29	Loliolide (1,3-dihydroxy-3,5,5-trimethylcyclohexylidene-4-acetic acid lactone)	$C_{11}H_{16}O_3$	196.24	Benzofuran
	24.44	88.34	Caffeine (1,3,7-trimethylxanthine)	$C_8H_{10}N_4O_2$	194.19	Purine alkaloid
	26.77	0.68	Palmitic acid (Hexadecanoic acid)	$C_{16}H_{32}O_2$	256.42	Fatty acid
RS	20.201	1.25	Di(n-octadecyl) phosphite	$C_{36}H_{74}O_3P+$	585.9	Ester
	34.356	23.80	Bis(2-ethylhexyl) phthalate	$C_{24}H_{38}O_4$	390.56	Phthalate
	27.102	2.33	1-Octadecene	C_{18} H_{36}	252.48	Alkene
	30.112	1.43	Trifluoroacetic acid, n-octadecyl ester	$C_{20}H_{37}F_3O_2$	366.5	Ester

Table S2. FT-IR spectral characteristics of RS and TL (before) and (after) Fe|Mn ions sorption

Wave number (cm^{-1})		Differences (D)	Assignment
RS	RS-Fe|Mn		
3,432.10	3,433.79	1.69	O-H stretching
2,923.00	2,923.00	0	C-H stretching
1,623.45	1,634.94	11.49	C=C stretching
1,318.23	1,321.18	2.95	C=O stretching
1,101.94	1,070.22	−31.72	C-OH stretching
Wave number (cm^{-1})		Differences (D)	Assignment
TL	TL-Fe|Mn		
3,420.07	3,433.20	13.13	O-H stretching
1,621.20	1,638.27	17.07	C=C stretching
1,445.83	1,382.98	−62.85	C=O stretching
1,107.02	1,066.48	−40.54	C-OH stretching
611.90	613.17	1.27	C-N stretching

D: The wave number difference in corresponding absorption peaks of samples, before and after Fe and Mn ions sorption

Table S3 Summary of the main parameters of Pareto design of GMDH-type neural network

Parameter	Value
Population size	200
Number of iteration	1,000
Mutation	0.08
Crossover	0.98
Number of the objective function	2.00
Number of hidden layers	5.00

Table S4. Training error and prediction error of design point in deterministic approaches

Outputs	Process	A		B		C	
		TE	PE	TE	PE	TE	PE
Out. Conc.	RS-Fe	0	0.118	0.003	0.008	0.001	0.040
	TL-Fe	0.022	0.406	0.042	0.095	0.024	0.207
	RS-Mn	0.002	0.842	0.016	0.019	0.004	0.187
	TL-Mn	0.035	0.372	0.046	0.074	0.038	0.182

Table S5. Developed structure of the GMDH-type-NN model with 4 and 5-hidden layers for the output concentration

Process	Inputs																T E	PE
TL-Fe	a	c	d	f	c	c	c	d	a	f	c	d	c	d	c	f	0.024	0.207
	a	d	b	f	b	b	b	d	b	b	f	g	b	c	f	f		
RS-Fe	a	c	e	f	a	d	b	d	a	d	g	g	c	d	d	d	0.001	0.040
	a	c	d	f	c	g	g	g	a	d	a	f	c	f	c	f		
	a	f	f	g	b	d	c	d	a	g	c	f	c	c	f	f		
	a	f	d	e	d	e	d	e	a	g	f	c	b	b	d	e		
TL-Mn	a	a	a	d	a	c	d	f	a	b	a	e	b	b	d	f	0.038	0.182
	a	a	b	c	a	f	b	b	a	b	a	f	c	f	g	g		
RS-Mn	a	c	d	f	a	d	a	d	b	b	b	c	e	e	f	g	0.004	0.187
	a	c	d	f	b	f	c	d	b	c	c	g	b	c	d	d		
	a	c	e	f	a	d	d	d	a	d	g	g	c	d	f	f		
	c	d	e	f	c	f	g	g	c	f	c	g	d	f	d	f		

a: Temperature (°C) b: pH — c: Concentration (mg/l) d: Adsorbent dosage (mg) e: Input flow rate (ml/min) f: Time (min) g: Output flow rate (ml/min)

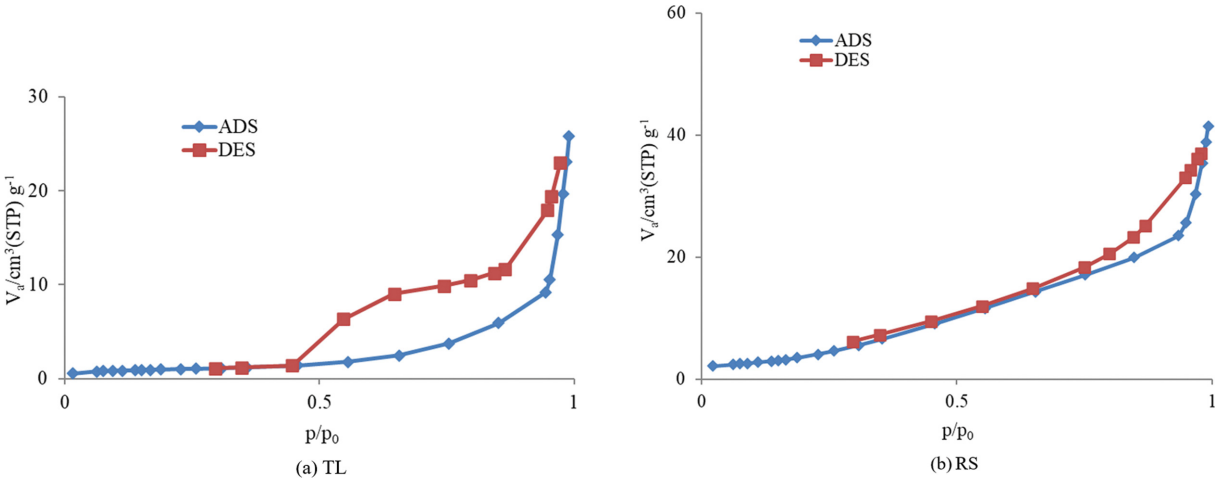

Fig. S1. Nitrogen adsorptions/desorption isotherms of TL and RS at −196.15 °C.

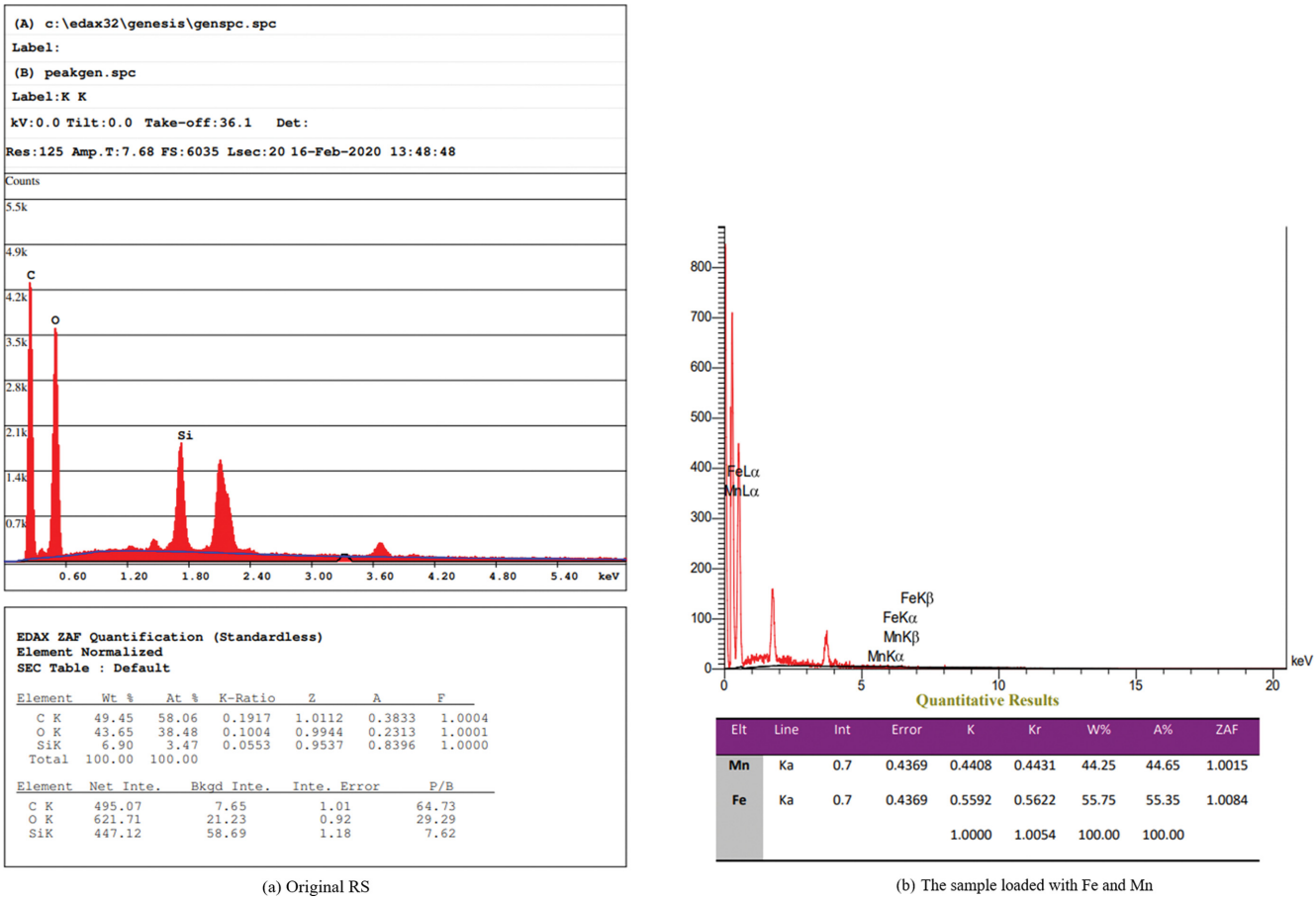

(a) Original RS

(b) The sample loaded with Fe and Mn

Fig. S2. The EDS spectra of RS samples.

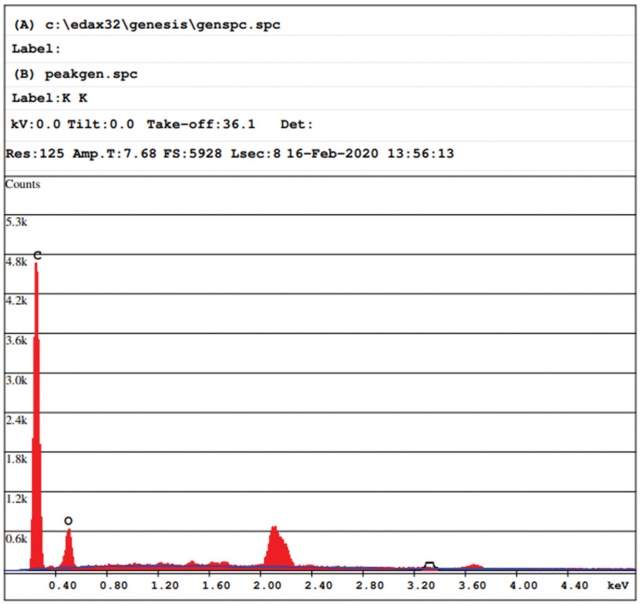

EDAX ZAF Quantification (Standardless)
Element Normalized
SEC Table : Default

Element	Wt %	At %	K-Ratio	Z	A	F
C K	74.62	79.66	0.5457	1.0042	0.7280	1.0002
O K	25.38	20.34	0.0440	0.9875	0.1757	1.0000
Total	100.00	100.00				

Element	Net Inte.	Bkgd Inte.	Inte. Error	P/B
C K	1283.30	11.42	0.98	112.33
O K	248.30	31.48	2.48	7.89

(a) Original TL

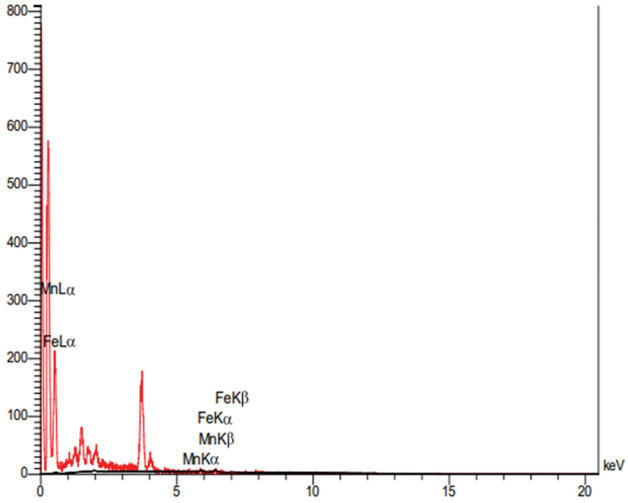

Quantitative Results

Elt	Line	Int	Error	K	Kr	W%	A%	ZAF
Mn	Ka	1.2	0.3909	0.4321	0.4345	43.37	43.78	1.0017
Fe	Ka	1.3	0.3909	0.5679	0.5709	56.63	56.22	1.0082
				1.0000	1.0054	100.00	100.00	

(b) The sample loaded with Fe and Mn

Fig. S3. The EDS spectra of TL samples.